PHOTONIC SENSORS / Vol. 10, No. 4, 2020: 306–315

2D and 3D Shape Sensing Based on 7-Core Fiber Bragg Gratings

Tianting LAI, Pu CHENG, Congliao YAN, Chi LI, Wenbin HU*, and Minghong YANG*

National Engineering Laboratory for Fiber Optic Sensing Technology, Wuhan University of Technology, Wuhan 430070, China

*Corresponding authors: Minghong YANG and Wenbin HU E-mail: minghong.yang@whut.edu.cn and wenbinhu_whut@163.com

Abstract: A fiber-optic shape sensing based on 7-core fiber Bragg gratings (FBGs) is proposed and experimentally demonstrated. The investigations are presented for two-dimensional (2D) and three-dimensional (3D) shape reconstruction by distinguishing bending and twisting of 7-core optical fiber with FBGs. The curvature and bending orientation can be calculated by acquiring FBG wavelengths from any two side cores among the six outer cores. And the shape sensing in 3D space is computed by analytic geometry theory. The experiments corresponding of 2D and 3D shape sensing are demonstrated and conducted to verify the theoretical principles. The resolution of curvature is about 0.1 m^{-1} for 2D measuring. The error of angle in shape reconstruction is about 1.89° for 3D measuring. The proposed sensing technique based on 7-core FBGs is promising of high feasibility, stability, and repeatability, especially for the distinguishing ability on the bending orientation due to the six symmetrical cores on the cross-section.

Keywords: Shape sensing; fiber Bragg gratings; multi-core fiber

Citation: Tianting LAI, Pu CHENG, Congliao YAN, Chi LI, Wenbin HU, and Minghong YANG, "2D and 3D Shape Sensing Based on 7-Core Fiber Bragg Gratings," *Photonic Sensors*, 2020, 10(4): 306–315.

1. Introduction

Shape sensing is of great practical significance in the safety monitoring of buildings and aircrafts, human motion monitoring, intelligent robot posture monitoring, intelligent material deformation monitoring, and other fields [1–3].

Shape sensing technology consists of two main categories, electrics and optics, both of which are realized by indirect or direct sensing via stress and strain measuring [4]. The fiber optic shape sensors (FOSSs), including fiber Bragg grating (FBG) on the multicore optical fiber (MCF) and optical frequency domain reflectometry (OFDR), attract more interest due to their inherent ability for distributed sensing [5–8]. The FOSSs based on the OFDR technique on normal fibers and fibers with continuous grating have been proposed [9–11]. The curvature sensitivity and spatial resolution for distributed shape sensing have been investigated [12]. In order to overcome the limitation of curvature measurement of single-core grating, in recent years, multi-core fiber has been used to measure shape, and the research of curvature sensing has attracted more and more attention [13–18]. In 2000, Gander *et al*. [19] used multi-core

Received: 27 November 2019 / Revised: 09 January 2020

DOI: 10.1007/s13320-020-0579-0
Article type: Regular

gratings to measure bending deformation, and the curvature error was 0.14 m^{-1}. In 2003, the curvature error measured by the similar method reached 0.047 m^{-1} [20]. In 2016, a twisted multi-core fiber grating with a length of more than 1 meter was used, and the OFDR technique was used to analyze the time difference and optical path difference of backward scattered light by 20 nm scanning near 1550 nm, and the spatial resolution of about 40 microns was achieved [21]. Recently, the 7-core multicore fiber, as well as the manufactural progress of the fan-in/fan-out, has been developed and fabricated widely. Compared with the other MCF, the 7-core MCF would be promising in shape sensing field due to the highly distinguishing ability on the bending orientation for the six symmetrical cores on the cross-section. Zhang *et al.* [22] has presented FBG inscribed in a trench-assisted heterogeneous 7-core fiber for bending sensing.

In this paper, we investigate the two-dimensional (2D) and three-dimensional (3D) shape sensing of 7-core FBGs. The theoretical calculation and simulation of bending and twisting are built in 2D space and 3D space. The experiments are then implemented to verify the shape sensing of 7-core fiber gratings. The shape in 3D space is finally reconstructed quantitatively.

2. Sensing mechanism analysis

The sensing mechanism of 7-core fiber gratings shape sensor of this investigation can be divided into two parts as described below.

2.1 2D Bending and twisting mechanism

The fiber grating bending sensing technology is based on its axial strain sensing characteristics. According to the coupled mode theory [23], the central wavelength of the fiber grating is determined by two parameters: the effective refractive index and the period of fiber grating. According to the mathematical model of FBG, the relative wavelength shift by strain of fiber gratings can be expressed as

$$\frac{\Delta\lambda}{\lambda}=(1-P_\varepsilon)\cdot\varepsilon \tag{1}$$

where λ is the central wavelength of FBG, $\Delta\lambda$ is the wavelength shift, ε is the axial strain applied on the grating, and P_ε is the photo-elastic coefficient related to the material.

Curvature of a substrate normally leads to a strain, which is one of the main parameters for FBG sensing. The bending sensing based on multicore fiber gratings is realized by measuring the curvature induced strain on FBG writing on different cores at the same position.

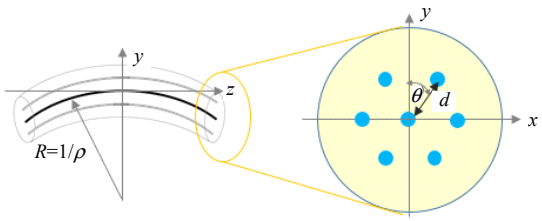

Fig. 1 Schematic diagram of 7-core optical fiber.

As shown in Fig. 1, the distance between the central core and the side core, normally denoted by pitch size, is d. After a bending of the fiber, assuming that the curvature radius of the core bending is R and the bending direction at the cross-section is equal to the forward direction of y-axis, the axial strain of any side core can be expressed as

$$\varepsilon=\pm\frac{d}{R}\cdot\cos\theta \tag{2}$$

where θ is the angle between the side core and y-axis at the cross-section. The positive and negative signs here are used for indicating the bending direction. The stretching of a fiber core is represented by a positive sign, while the compressing by a negative sign. The central core will not be affected by the bending of fiber. Significantly, the wavelength shift error caused by temperature can also be compensated because the central core and the side core are in the same environment with a same fiber cladding [24]. The linear relationship between the bending curvature

and wavelength shift of the optical fiber can be expressed as

$$\Delta\lambda_n - \Delta\lambda_1 = kd\rho\lambda_n \cos\theta_n,\ n = 2,\ 3,\ \cdots,\ 7 \quad (3)$$

where $\Delta\lambda_n$ is the wavelength shift of side core and $\Delta\lambda_1$ is the wavelength shift of central core; $\rho = 1/R$ is the curvature of bending; $k = (1 - P_\varepsilon)$ is the longitudinal strain sensitivity coefficient which is 0.784 for standard silica fibers; λ_n is the wavelength of the FBGs in the MCF at a free state. For the sake of convenient calculation, the positive and negative signs have been removed, and the θ_n ranges from –180° to 180°.

When the wavelength shift has been detected, by using the data of central core (denoted by 1) and any two side cores (denoted by m and n), the angle between each core and bending direction, and the curvature of the fiber can be deduced as

$$\theta_n = \left(1 - \frac{|\Delta\lambda_n|}{\Delta\lambda_n}\right)\pi + \arctan\left(\frac{1}{\tan(m-n)\pi/3} - \frac{\lambda_n(\Delta\lambda_m - \Delta\lambda_1)}{\lambda_m(\Delta\lambda_n - \Delta\lambda_1)\sin((m-n)\pi/3)}\right),$$
$$m,\ n = 2,\ \cdots,\ 7 \quad (4)$$

$$\rho = \frac{\Delta\lambda_n - \Delta\lambda_1}{kd\lambda_n \cos\theta_n} = \frac{\Delta\lambda_n - \Delta\lambda_1}{K} \quad (5)$$

where m and n represent different side cores. Here, K is introduced as the hybrid coefficient of the curvature measuring.

The two equations above can reconstruct the bending and torsion of optical fiber quantitatively by analyzing the wavelength shift of 7-core FBGs. It can be easily derived that the 7-core FBGs can exhibit a good distinguishing ability on the bending orientation owing to the six symmetrical cores on the cross-section.

2.2 3D shape sensing mechanism

In order to achieve shape sensing in 3D space, it is necessary to initialize the core distribution of the optical fiber. FBGs with different central wavelengths need to be inscribed evenly on the optical fiber. Figure 2 shows the theoretical model of shape sensing. As shown in Fig. 2, assume that the optical fiber is initially located along z-axis, and the fiber starts at the coordinate origin, i.e., the curvature of the first segment, arc ab, defines the local coordinate for the following calculation. FBGs are inscribed at the midpoint of each segment of fiber, such as 1st segment, arc ab and 2nd segment, arc bc, with a fixed length of L_n. It is assumed that the length is short enough where only one homogeneous bending occurs. φ_1 is the intersection angle of y-axis and the projection of fiber on the x-y surface during the first bending. γ_1 and γ_2 are the central angle of arc ab and arc bc. Then multistage curvature in 3D space can be theoretically modeled.

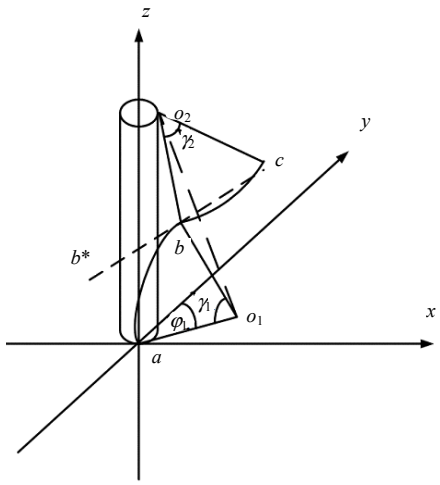

Fig. 2 Shape sensing theoretical model.

Under the defined coordinates, arc ab is tangent with z-axis and o_1 is the center of arc ab. Segment ao_1 is on the x-y surface and indicates the bending direction. According to (4), the intersection angle between the bending direction and each side core can be calculated. We choose side core 2 as the direction of y-axis, then φ_1 is equal to θ_2. According to (5), the curvature can be calculated, so γ_1 is equal to ρ multiplied by L_1.

Based on the coordinates of a, b, and o_1 built from the first segment, the curvature of the second segment can be sequentially computed by solving the equation of tangent of arc ab at point b. Assuming b^* is a point on the tangent, according to the space tangent equation formula, the equation of line bb^* can be described as

$$\frac{x-b_x}{2C_1b_y-2C_1o_{1y}-2B_1b_z+2B_1o_{1z}}=\frac{y-b_y}{2A_1b_z-2A_1o_{1z}-2C_1b_x+2C_1o_{1x}}=\frac{z-b_z}{2B_1b_x-2B_1o_{1x}-2A_1b_y+2A_1o_{1y}} \quad (6)$$

where (A_1, B_1, C_1) is the normal vector of plane abo_1. b_x, b_y, and b_z are the coordinates of x, y, and z axes at point b, and o_{1x}, o_{1y}, and o_{1z} are the coordinates of x, y, and z axes at point o_1. For the convenience of calculation, the precise position of b^* is defined as long as (6) is solved.

As for arc bc, the trace of the 2nd segment, bb^* is also regarded as its tangent component. The angle between bo_1 and bo_2 is $(\theta_2-\varphi_1)$. Then the coordinate of o_2 can be described by (7)–(9):

$$|bo_2|=\frac{1}{\rho_2}. \quad (7)$$

$$\mathbf{bb}^*\cdot\mathbf{bo}_2=0. \quad (8)$$

$$\theta_2-\varphi_1=\arccos\left(\frac{\mathbf{bo}_1\cdot\mathbf{bo}_2}{|bo_1||bo_2|}\right) \quad (9)$$

and the coordinate of c can also be described by (10)–(12):

$$|co_2|=\frac{1}{\rho_2} \quad (10)$$

$$|bc|=\frac{2}{\rho_2}\cdot\sin\left(\frac{\rho_2L_2}{2}\right) \quad (11)$$

$$A_2(c_x-b_x)+B_2(c_y-b_y)+C_2(c_z-b_z)=0 \quad (12)$$

where (A_2, B_2, C_2) is the normal vector of plane bb^*o_2. Point c is also on the plane bb^*o_2. L_2 is the length of arc bc.

In this case, all the information in the curvature of second segment bc has been obtained. For the coming curvature of cd, de, and so on, we can use this recurrence relation to obtain the information of all the points. In this way, the shape of optical fiber is reconstructed.

3. Device fabrication and experiments

3.1 Shape sensor optical assembly

7-core optical fiber with a hexagonal distribution is used in this paper. The cross-section of the MCF is shown in Fig. 3, with a cladding diameter of 150 μm, a mode field diameter (MFD) of 9.5 μm, and a pitch size of 41.5 μm. The inter-core crosstalk is suppressed to be less than –45 dB, which coincides with the requirements of spatial division multiplexing communication and shape sensing. The FBGs are inscribed in 7-core MCF on a FBG writing system with 248 nm excimer laser. The FBG spectra of different cores are shown in Fig. 4. The difference of the central wavelength among the cores is caused by the nonhomogeneous distribution of laser energy in different cores while FBG is being written to the fiber, which has been shown as a trivial effect on the wavelength interrogation and readout. In the following analysis and discussion, all the central wavelengths of side cores are normalized in accordance with the value of the central core.

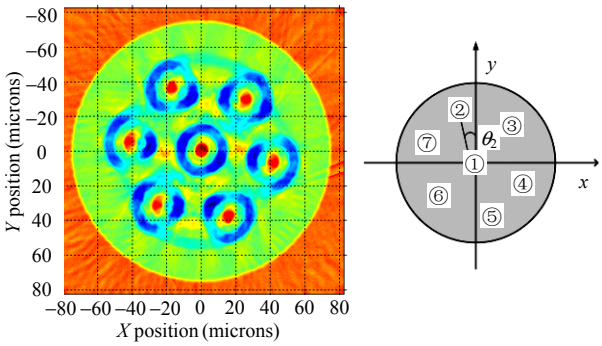

Fig. 3 Refractive index profile of 7-core optical fiber.

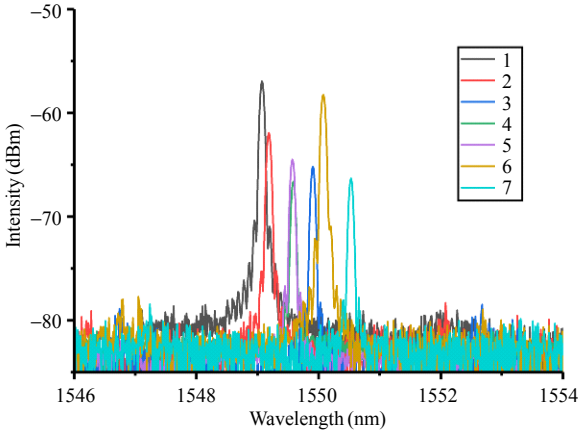

Fig. 4 Spectrum of 7-core FBGs.

3.2 2D curvature measuring system

The experimental setup for 2D curvature measurements is shown in Fig. 5. The components

include 7-core FBGs, a fan-in-fan-out device, deformation device, a multi-channel FBG interrogator system with a resolution of 1 pm, and a processing computer. The interrogator provides the recording of multiple channels simultaneously with a frequency of 100 Hz and resolution of 1 pm. One end of the MCF fiber is coupled with the fan-in-fan-out device, and the other end is inserted into alcohol solution to suppress the back reflection from the end-face. The seven fiber jumpers of the fan-in-fan-out device are connected to the seven channels of the interrogator. Then the wavelength data obtained by the interrogator are collected in the computer and the bending curve is reconstructed by a processing program based on the theoretical principles presented in the previous section.

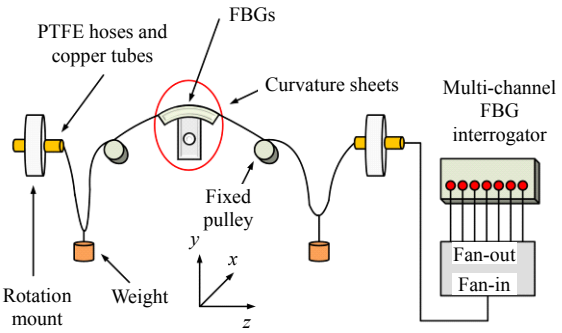

Fig. 5 Experimental setup for 2D curvature measurement.

As shown in Fig. 5, a series of components is assembled to fix the MCF. Experiments are implemented to build the relationship between the 2D curvature and the FBG wavelength shift by varying the curvature producer, an arc-like curvature sheet shown in the middle of Fig. 5. A series of curvature sheets (with curvature ranging from 0 m^{-1} to 20 m^{-1}) is used to produce precise curvatures in the (yz)-plane and the curvatures are applied on a FBG in the MCF. The Poly tetra fluoroethylene (PTFE) hoses and copper tubes on both sides of the FBG are used to ensure that the FBG position locates exactly on the curvature sheet without any displacement. Two weights are hung between the pulley and the rotation mount to assist the FBG immobilization. During the 2D bending experiment, it is important to constraint the torsion when the curvature sheet is changed, with the purpose to verify the theory of 2D curvature. Two weights ensure the tightness of fiber without torsion.

3.3 3D shape measuring system

A top-view diagram of the experimental setup for 3D shape measurements is shown in Fig. 6. The 3D experimental system is different from the 2D system by the introduction of the torsion joint, which locates between two 2D setups. In this case, the bending in three directions in 3D space can be produced respectively. The whole setup can be divided into three parts, two 2D setups (denoted by Part 1 and Part 3) with vertical but oppositely orientation of bending, and separated by a cylindrical holder (denoted by Part 2) to produce horizontal bending. It is noted that the pushing directions of these three parts are orthogonal to each other. The bending of the two 2D setups is accomplished by the arc-like curvature sheet, as same as that shown in Fig. 5. For Part 3, the bending is conducted by the pulley fixed on the joint cylindrical holder, varying from 5 m^{-1} to 8 m^{-1}. Three FBGs inscribed in the MCF, as marked in Fig. 6, are employed to build the relationships between the wavelength responses and the bending along three orthogonal directions. The central wavelengths of three FBGs are 1542 nm, 1546 nm, and 1550 nm, respectively. The spacing of FBGs is 0.1 m.

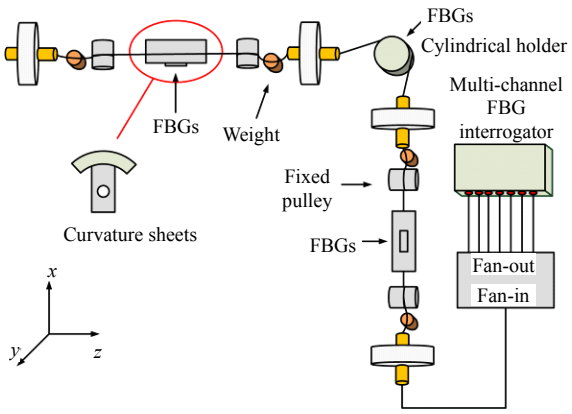

Fig. 6 Experimental setup for 3D curvature measurement.

4. Results and discussion

4.1 Results of 2D curvature measurement

The wavelength of the FBG in the MCF was monitored by using the multi-channel interrogator on the 2D curvature measuring setup shown in Fig. 5. By varying the curvature of sheets from 0 m^{-1} to 20 m^{-1}, the spectrum of three side cores was observed as moving toward longer wavelength, i.e., red shift. Meanwhile, the spectrum of the other three side cores was observed as moving toward shorter wavelengths, i.e., blue shifts. And the spectrum of central core has remained unchanged. The wavelength shifts of FBGs in the seven cores at different curvature are shown in Fig. 7. All of the wavelength shifts of side cores had already been compensated by central core to eliminate the influence of extra strain caused by the weights and other factors.

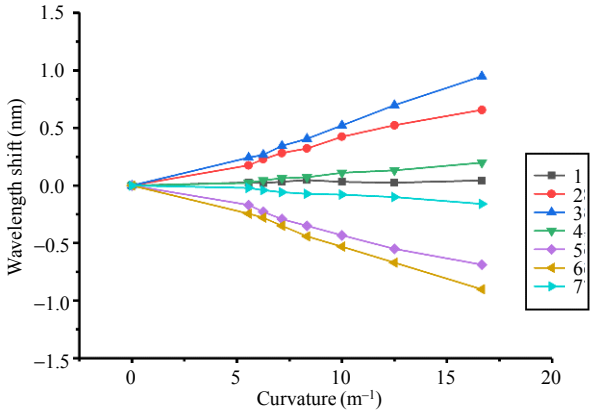

Fig. 7 Central wavelength shift of seven cores during the curvature sensing experiment.

From Fig. 7, it can be found that the side core 3 and side core 6 have the biggest curvature sensitivity. The side cores 2, 3, and 4 have shown red shift of wavelength while the side cores 5, 6, and 7 have shown blue shift, which infers the stretch of cores 2, 3, and 4 and the compress of cores 5, 6, and 7.

According to (4) and (5), as long as the data of Bragg wavelength shift have been obtained, the position of each core corresponding to the bending direction and the curvature of the fiber can be deduced. To illustrate the orientation of the cross-section of the MCF more precisely, the wavelength shifts of each cores are analyzed.

Table 1 shows the average curvature sensitivity of each core, which was obtained by linear fitting. According to (5), the slope of the wavelength shift can be interpreted as the hybrid coefficient (K) of the curvature measuring. It is obvious that the absolute values of the slopes of side core 2 and side core 5 are close, which implies the opposite states of the two cores, stretching (denoted by positive sign) and compressing (denoted by negative sign) states. The same cases can be found for side cores 3 and 6, side cores 4 and 7.

Table 1 Linear fitting statistics.

Core	Value of slope (nm/m^{-1})
Central core 1	0.00217
Side core 2	0.04131
Side core 3	0.05873
Side core 4	0.01258
Side core 5	–0.04362
Side core 6	–0.05564
Side core 7	–0.00971

We substituted slope to (5). n took a value of 2 while m took values of 3, 4, 6, and 7. Then we could get four values of θ_2: –46.78°, –42.89°, –44.35°, and –40.32°. The average value of θ_2 is –43.585°. Figure 8 demonstrates the estimated position of each core during the bending process. According to the resolution of multi-channel interrogator, the theoretical minimum curvature can reach 0.2 m^{-1}. From the experiment, we considered the resolution of curvature was about 1 m^{-1} due to the external interference at interrogator. The orientation error was about 1.98°.

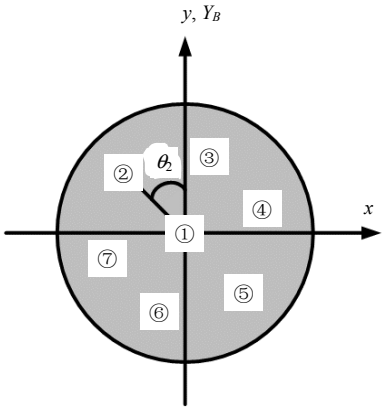

Fig. 8 Cross-section of optical fiber.

By adjusting two rotation mounts simultaneously on both sides of the FBG and curvature sheets, the bending orientation of optical fiber can be altered from 0° to 360°. The wavelength shifts of seven cores versus the altered angle are plotted in Fig. 9. The trend of wavelength shift is an obvious sinusoidal curve, which is consistent with (5).

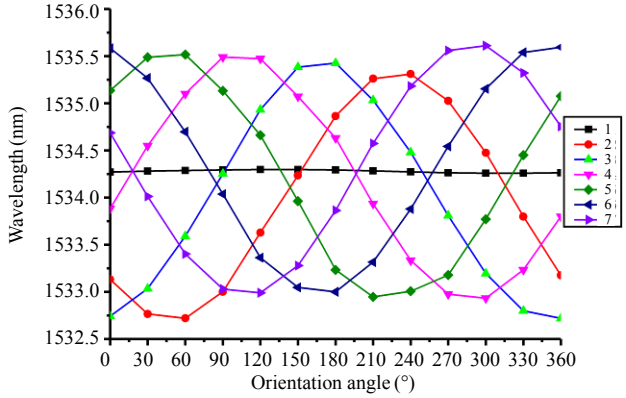

Fig. 9 Bragg wavelength shifts at different bending orientations.

In the next experiment, the curvature sheets are pushed toward the MCF to produce the bending on the FBG. The pushing is conducted by a motorized linear stage assembled with the curvature sheets. We have investigated the influence of the change of pushing height of the curvature sheet on the wavelength shift of FBG. Figure 10 demonstrates the wavelength shift of six-side cores after compensation of the central core. As a result, the error of pushing height by using the mechanical device can be almost ignored.

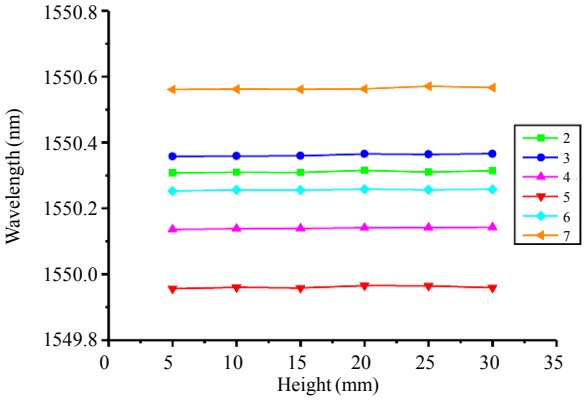

Fig. 10 Wavelength shift of six side cores versus the pushing height after compensation of central core.

4.2 Results of 3D curvature measurement

The wavelength shift of the three FBGs corresponding to three orientations versus different curvatures are shown in Fig. 11. Similar to the results shown in Fig. 7, the wavelength shifts for all of the three orientations are linearly related to the curvature. For the first and the third part of the deformation device, the curvature of the sheets varies from 2.5 m^{-1} to 20 m^{-1}, and for the curvature of fixed pulley of the second part, it varies from 5 m^{-1} to 8 m^{-1}.

For the first part, the wavelengths of side cores 2, 3, and 7 have presented red shift, and cores 4, 5, and 6 blue shift, whereas opposite case occurs for the third part, as shown in Figs. 11(a) and 11(c). This can be explained by the opposite moving direction of linear traveling stages in the two parts during the experiments. For both cases, the wavelength of central core remains unchanged. According to (4) and (5), the orientation of the seven cores can be mapped, as shown in the insets of Figs. 11(a) and 11(c).

Figure 11(b) shows the wavelength shift for the second part of the deformation device. By varying the curvature of fixed pulley from 5 m^{-1} to 8 m^{-1}, the spectra of side cores 3, 4, and 5 were observed as moving toward longer wavelengths, i.e., red shifts. The inset of Fig. 11(b) presents the orientation accordingly.

Linear fitting was employed to get the average curvature sensitivity of each core, i.e., the slope of the plot. According to (4), the value for each case can be calculated. Three average values of θ_2 at three parts of the deformation device are –22.45°, –110.56°, and 160.73°. The difference between two orientations is 88.11 and 271.29, which is consistent well with the orthogonal moving direction applied on the three FBGs. It can be concluded that the orientation errors of the estimation are 1.89° and 1.29°.

To verify the effectiveness of the 3D shape sensing arithmetic, we used a program to solve coordinates of different segments of the fiber according to (7)–(12). The coordinate of a is (0, 0, 0)

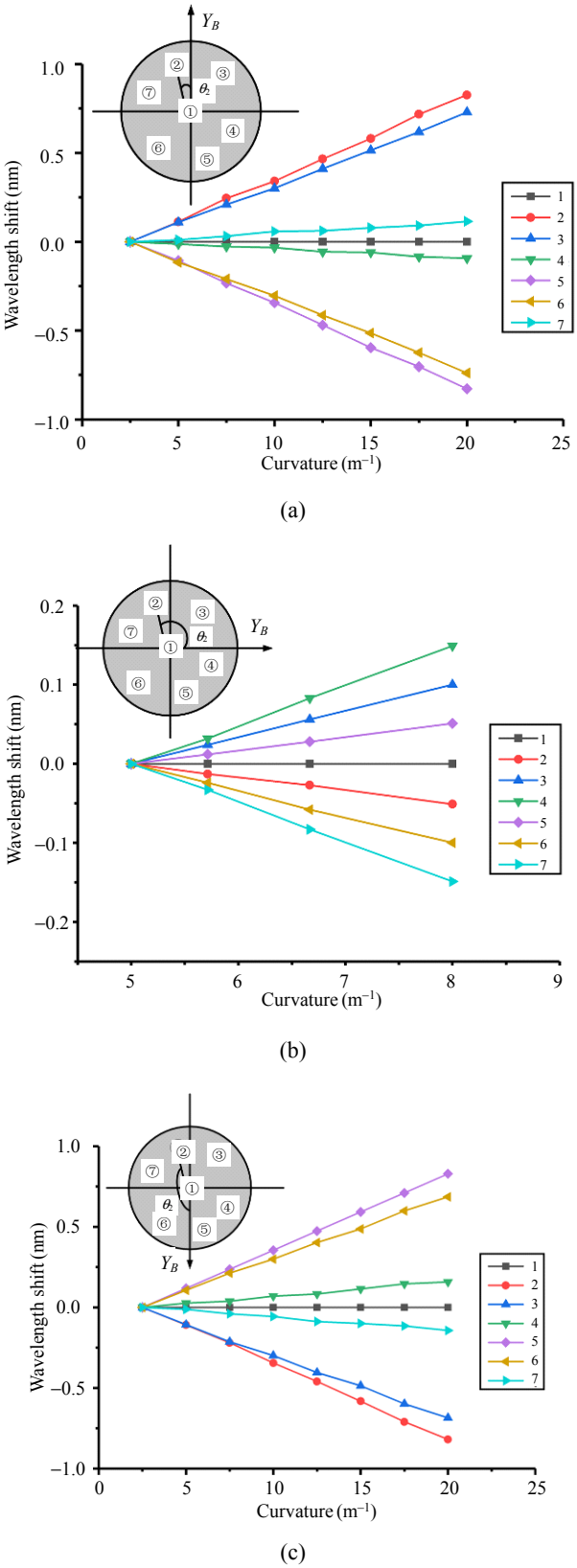

Fig. 11 Central wavelength shift of seven cores during the curvature sensing of (a) Part 1, (b) Part 2, and (c) Part 3 of the deformation device.

and the coordinates of b, c, and d solved by the program are (–0.009, 0.023, 0.096), (0.009, 0.106, 0.211), and (0.052, 0.175, 0.268). The bending condition of the fiber is shown in Fig. 12(a). The calculation of mathematical relationship between plane abo_1, bco_2, and cdo_3 shows that they are orthogonal with each other. As shown in Fig. 12(b), the simulation of shape sensing in the 3D space is almost in accordance with the space design of deformation device. And the curvature is the same in simulation and experiment. However, there are still some errors in the reconstruction because the length of each segment of fiber used is not short enough to ensure the smoothness at the junction.

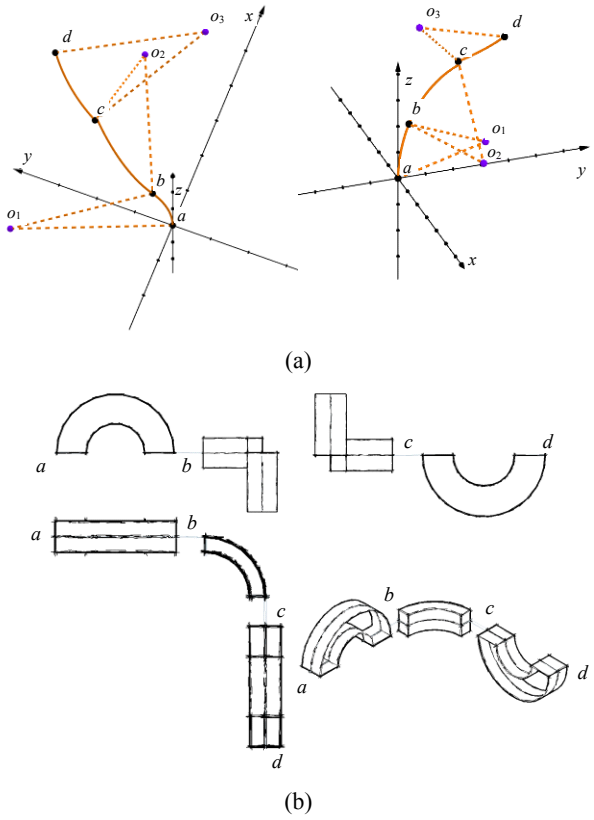

Fig. 12 Comparison of 3D position between the simulation and experiment: (a) the simulation of shape sensing in 3D space observed from different perspectives and (b) the experimental position of shape sensing in 3D space.

5. Conclusions

In conclusion, we propose and experimentally demonstrate a shape sensor based on 7-core fiber gratings. The mechanism and the theoretical

principles of the bending and twisting in 2D space and 3D space are discussed. Accordingly, the experimental setups for 2D and 3D are demonstrated. The effect of ambient temperature changes in the real applications of those systems can be compensated because the central core and the side core are in the same environment with the same fiber cladding. During the 2D experiment, the wavelength responses of the seven cores are studied by varying curvature without torsion and by rotating the holder under fixed curvature. The slope of the wavelength shift provides the hybrid coefficient of the curvature measuring. In the 3D experiment, three orthogonal stresses are applied on three FBGs in the setup to produce three of the bending directions. By acquiring the slopes of the three wavelength responses, the orientation angles are estimated to be –22.45°, –110.56°, and 160.73° for the three FBGs, with a maximum error of 1.89°. Owing to six symmetrical cores on the cross-section, the proposed fiber-optic shape sensing system has the advantages of high feasibility, stability, and repeatability, especially for the distinguishing ability on the bending orientation.

Acknowledgment

This work was supported in part by Major Technique Innovation Program of Hubei Province of China (Grant No. 2018AAA016) and the National Natural Science Foundation of China (NSFC) (Grant No. 61575151).

References

[1] E. M. Lally, M. Reaves, E. Horrell, S. Klute, and M. E. Froggatt, "Fiber optic shape sensing for monitoring of flexible structures," *Proceedings of SPIE*, 2012, DOI: 10.1117/12.917490.

[2] P. E. Dupont, J. Lock, B. Itkowitz, and E. Butler, "Design and control of concentric-tube robots," *IEEE Transactions on Robotics*, 2010, 26(2): 209–225.

[3] M. Gherlone, P. Cerracchio, M. Mattone, M. D. Sciuva, and A. Tessler, "Shape sensing of 3D frame structures using an inverse finite element method," *International Journal of Solids & Structures*, 2012, 49(22): 3100–3112.

[4] S. S. Kwon, W. K. Hong, G. Jo, J. S. Maeng, T. W. Kim, S. H. Song, *et al*., "Piezoelectric effect on the electronic transport characteristics of ZnO nanowire field-effect transistors on bent flexible substrates," *Advanced Materials*, 2010, 20(23): 4557–4562.

[5] C. R. Liao, D. N. Wang, and X. Fang, "Femtosecond laser fabricated fiber Bragg grating in microfiber for refractive index sensing," *Optics Letters*, 2010, 35(7): 1007–1009.

[6] C. S. Baldwin, T. J. Salter, and J. S. Kiddy, "Static shape measurements using a multiplexed fiber Bragg grating sensor system," *Proceedings of SPIE*, 2004, DOI: 10.1117/12.538091.

[7] T. Guo, Q. Zhao, Q. Dou, H. Zhang, L. Xue, G. Huang, *et al*., "Temperature- insensitive fiber Bragg grating liquid-level sensor based on bending cantilever beam," *IEEE Photonics Technology Letters*, 2005, 17(11): 2400–2402.

[8] A. Rauf, J. Zhao, B. Jiang, Y. Jiang, and W. Jiang, "Bend measurement using an etched fiber incorporating a fiber Bragg grating," *Optics Letters*, 2013, 38(2): 214–216.

[9] S. Wang, X. Fan, Q. Liu, and Z. He, "Distributed fiber-optic vibration sensing based on phase extraction from time-gated digital OFDR," *Optics Express*, 2015, 23(26): 33301.

[10] S. Loranger, M. Gagné, V. Lambiniezzi, and R. Kashyap, "Rayleigh scatter based order of magnitude increase in distributed temperature and strain sensing by simple UV exposure of optical fibre," *Scientific Reports*, 2015, 5: 11177.

[11] J. Bos, J. Klein, M. Froggatt; E. Sanborn, and D. Gifford, "Fiber optic strain, temperature and shape sensing via OFDR for ground, air and space applications," *Proceedings of SPIE,* 2013, DOI: 10.1117/12.538091.

[12] M. Amanzadeh, S. M. Aminossadati, M. S. Kizil, and A. D. Rakić, "Recent developments in fibre optic shape sensing," *Measurement*, 2018, 128: 119–137.

[13] I. Floris, S. Sales, P. A. Calderón, and J. M. Adam, "Measurement uncertainty of multicore optical fiber sensors used to sense curvature and bending direction," *Measurement*, 2019, 132: 35–46.

[14] D. Sebastian, L. Ines, B. Martin, S. Ron, K. Jens, S.

Kay, *et al*., "Multicore fiber with integrated fiber Bragg gratings for background-free Raman sensing," *Optics Express*, 2012, 20(18): 20156–20169.

[15] M. J. Gander, W. N. Macpherson, R. Mcbride, J. D. C. Jone, L. Zhang, I. Bennion, *et al*., "Bend measurement using Bragg gratings in multicore fiber," *Electronics Letters*, 2000, 36(2): 120–121.

[16] W. N. Macpherson, G. M. H. Flockhart, R. R. J. Maier, J. S Barton, J. D. C. Jones, D. Zhao, *et al*., "Pitch and roll sensing using fibre Bragg gratings in multicore fiber," *Measurement Science and Technology*, 2004, 15(8): 1642.

[17] J. Cui, K. Feng, J. Li, and J. Tan, "Development of a double fiber probe with a single fiber Bragg grating for dimensional measurement of microholes with high aspect ratios," *Optics Letters*, 2014, 39(10): 2868–2871.

[18] S. Werzinger, S. Bergdolt, R. Engelbrech, T. Thiel, and B. Schmauss, "Quasi-Distributed fiber Bragg grating sensing using stepped incoherent optical frequency domain reflectometry," *Journal of Lightwave Technology*, 2016, 34(22): 5270–5277.

[19] M. J. Gander, W. N. Macpherson, R. Mcbride, J. Jones, "Bend measurement using Bragg gratings in multicore fibre," *Electronics Letters*, 2000, 36(2): 120.

[20] G. M. H. Flockhart, W. N. Macpherson, J. S. Barton, J. D. C. Jones, L. Zhang, and I. Bennion, "Two-axis bend measurement with Bragg gratings in multicore optical fiber," *Optics Letters*, 2003, 28(6): 387–389.

[21] M. Hou, K. Yang, J. He, X. Xu, S. Ju, K. Guo, *et al*., "Two-dimensional vector bending sensor based on 7-core fiber Bragg gratings," *Optics Express*, 2018, 26(18): 23770–23781.

[22] H. Zhang, Z. Wu, P. P. Shum, R. Wang, X. Q. Dinh, S. Fu, *et al*., "Fiber Bragg gratings in heterogeneous multicore fiber for directional bending sensing," *Journal of Optics*, 2016, 18(8): 085705.

[23] W. P. Huang and J. Mu, "Complex coupled-mode theory for optical waveguides," *Optics Express*, 2009, 17(21): 19134–19152.

[24] W. Zhang, F. Li, and Y. Liu, "FBG pressure sensor based on the double shell cylinder with temperature compensation," *Measurement*, 2009, 42(3): 408–411.